International Journal of Fluid Machinery and Systems
Vol. 6, No. 2, April-June 2013

DOI: http://dx.doi.org/10.5293/IJFMS.2013.6.2.094
ISSN (Online): 1882-9554

Original Paper (Invited)

Design and Prediction of Three Dimensional Flows in a Low Speed Highly Loaded Axial Flow Fan

Xuejiao Liu, Liu Chen, Ren Dai and Ailing Yang

School of Energy and Power Engineering, University of Shanghai for Science and Technology
516 Jungong Road, Shanghai, 200093, China
lxj_0627@163.com, chen_liu@usst.edu.cn, dairen@usst.edu.cn, alyang@usst.edu.cn

Abstract

This paper describes the design to increase the blade loading factor of a low speed axial flow fan from normal 0.42 to highly loaded 0.55. A three-dimensional viscous solver is used to model the flows in the highly-loaded and normal loaded stages over its operation range. At the design point operation the static pressure rise can be increased by 20 percent with a deficit of efficiency by 0.3 percent. In the highly loaded fan stage, the rotor hub flow stalls, and separation vortex extends over the rotor hub region. The backflow, which occurs along the stator hub-suction surface, changes the exit flow from the prescribed axial direction. Results in this paper confirm that the limitation of the two dimensional diffusion does not affect primarily on the fan's performance. Highly loaded fan may have actually better performance than its two dimensional design. Three dimensional designing approaches may lead to better highly loaded fan with controlled rotor hub stall.

Keywords: highly-loaded fan, numerical simulation, stage loading factor

1. Introduction

Air cooling is an important technique in large electric motors and power generators to remove the inside heating from electric-magnetic stator. It is important to keep generator inside temperature under limitation for safety and efficiency. Cooling air is usually supplied with one multi-stage axial flow fan which can provide required pressure rise capacity with flexible combination of stages. It is motor designer's wish to reduce the number of fan stages and then to reduce motor shaft length for shaft stiffness and vibration considerations. This can be achieved by either increasing the blade speed or by increasing the stage load coefficient. Since fan is fixed with motor shaft, the blade speed is limited by the motor rotation speed which is usually 3000 or 1500 rotations per minute (RPM). A higher pressure rise will require increased stage loading.

The "Smith Chart" is a commonly used rule of thumb to plot compressor duty which indicates flow efficiency via the stage loading factor against the design flow coefficient. Best design zone locates for the loading factor of 0.4 and flow coefficient of 0.5. However the stage loading factor does not imply the aerodynamic difficulty in achieving high pressure rise. Wennerstrom [1] explains clearly that the work per stage is proportional to the change in absolute swirl velocity across the rotor. This permissible change is however limited by some loading parameter associated with boundary layer separation, which is so-called Lieblein criterion [2]. His result was that the static pressure rise coefficient should be less than 0.6.

With the development of CFD calculation capacity, the three-dimensional flows in turbomachinery can be computed and captured, which promotes the development of the high-turning angle blade technology. Controlled diffusion airfoils become available by airfoil optimal design technology. Emmerson [3] successfully modeled the C148 transonic fan using the fully three-dimensional Reynolds-averaged Navier-Stokes code at the design condition. The stator turning angle of C148 was over 57 degrees. The result of numerical simulation showed good qualitative agreement with measurements in all regions of the flow field. His research improved design methodologies for future highly loaded single and multistage fans.

Calvert etc. [4] designed, tested and analyzed a highly loaded transonic fan stage. The maximum turning angle of the newly designed blade was close to 60 degrees at the stator hub. The performance reached close to the requirement of design. The project was successful in establishing a logical design procedure for modern, multistage fans by linking 1D stage-stacking concepts and detailed CFD-based methods.

Friedrichs etc. [5] studied experimentally the stator hub and blade flow in two different stators of a highly loaded single-stage axial-flow low-speed compressor. The stator turning angle was also over 60 degrees. In the hub corner separation flow on the

Received September 29 2012; revised January 20 2013; accepted for publication February 28 2013: Review conducted by Prof. Hyung-Hee Cho. (Paper number O13005S)
Corresponding author: Xuejiao Liu, Professor, lxj_0627@163.com

This paper was presented at 5th International Symposium on Fluid Machinery and Fluids Engineering, October 24-27, 2012, Jeju, Korea.

suction surface was evidently found. Flow separation was delayed when the stator hub region was redesigned with forward swept. Testing results showed that the surge margin was increased and the efficiency improved by about 10 percent especially at small mass flow rate conditions.

Sonoda etc. [6] used evolutional optimization methods to redesign a high turning compressor airfoil at low Reynolds numbers with CFD calculation method. Schreiber etc. [7] further tested the new airfoil and proofed its aerodynamic performance improvements. It was showed that high turning airfoil in diffusion flow was possible to break through Lieblein limit when it was aerodynamically optimized. Dickens and Day [8] provided a more general study of the problems with high loading. They suggested that increasing rotor loading showed better able to tolerate flow separation than the stator for increasing the stage loading.

Most of the highly loaded designs in literature discussed above concern attempts to design for high speed axial flow fans, in which the flow mach number is larger than 0.5 and flow's compressibility has important effects. The purpose of current work is to provide a computational study of a highly loaded design for low speed axial flow fan, where flow is regarded as incompressible. Possibility to design a low speed highly loaded axial fan close to the Lieblein diffusion limitation is studied. Three dimensional flows in normal loaded fan (NLF) and highly loaded fan (HLF) designs are calculated and compared to find the limit of fan load. Results will explain the loss resources. Flow fields in rotor and stator will give indications to further research directions to improve the HLF efficiency.

2. Designing Approach

2.1 Design of highly loaded stage

One normal axial fan with loading coefficient of 0.42 is referred as the baseline fan. Its airfoil camber angle of rotor is 17° and stator 39° respectively. The study aim is to increase the fan's loading for 30 percent at its design condition which means a new fan stage having loading coefficient of 0.55. Designing constraint is the mass flow rate will be maintained. As Wennerstrom [1] indicated, the only way to increase stage loading is to increase the stage's absolute velocity swirl when the blade rotation speed is limited. As shown in Fig.1, the stage inlet flow angle is kept as axial, increased absolute velocity C2 will bring up larger flow deflections in both rotor and proceeding stator. The stator outlet flow angle is designated to be the same as the rotor absolute inlet flow angle to satisfy the requirement of the repeating stage for multi-stage designing. Simple numeric calculation upon Fig.1 resulted that the new rotor camber angle was increased to 24° and the new stator camber angle was increased up to 53°.

From Fig.1, it is evident that newly designed fan will have larger flow deflection or high turning across rotor and stator. Flow losses will also be increased and fan's efficiency will be decreased. Before its further realization, some criterions have to be found to evaluate new design's feasibility. Different factors had been developed in literature, among which Lieblein diffusion factor is the most common referred one.

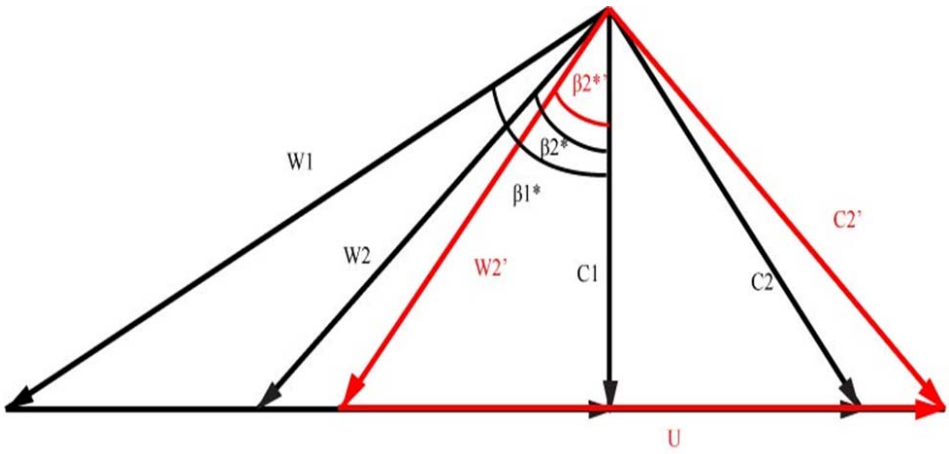

Fig. 1 Velocity diagrams for normal and highly loaded fans

Lieblein[2] developed one of the first and most commonly used measures of the adverse pressure gradient experienced by the suction surface boundary layer; the diffusion factor. It can be defined as follows:

$$DF_{Lieb} = (1 - \frac{\cos\beta_1^*}{\cos\beta_2^*}) + \frac{\cos\beta_1^*}{2b/t}(\tan\beta_1^* - \tan\beta_2^*) \quad (1)$$

The diffusion factor is strictly controlled within 0.6 in a fan. This is because the diffusive flow accompanied with large deflection is more easily suffered from boundary-layer separation along blade suction side. The limitation of diffusion factor is defined at flow loss is twice of the minimum value. Beyond this limit, flow in compressor blade row is regarded as a stalled one. Although Lieblein diffusion factor is simple, it provides a useful tool at the primary step of fan design to evaluate designing feasibility. Certainly it does not give any prediction and explain of performance decoration.

The diffusion factors of both fan rotors and stators are calculated from the eq. (1) and their values are listed in Table 1. NLF fan had moderate diffusion factor for rotor and stator. HLF has now higher diffusion factors which are closer to Lieblein criteria of

0.6. It can be derived that HLF will have increased pressure rise but will suffer efficiency decrease. It is now interesting to identify whether HLF performance can be acceptable over its operation range. It is also attractive to know its detailed flow structure to find reasoning of the deficiency.

Table 1 Profile parameters and diffusion factor

Profile parameters	b [mm]	t [mm]	β_1^* [°]	β_2^*(') [°]	DF_{Lieb}
Rotor(NLF)	46.22	27.43	61.91	46.30	0.43
Stator(NLF)	41.32	22.51	36.21	0	0.35
Rotor(HLF)	44.54	27.43	61.91	42.26	0.50
Stator(HLF)	42.09	22.51	46.04	0	0.50

2.2 Design of blade airfoil

The blade airfoil of axial fan/compressor is usually selected from standard NACA65 or C4 series airfoils. Special camber is built with respect to airfoil lift coefficient. Blade airfoil is then constructed by imposing prescribed thickness distribution upon the designated camber line. At low speed flow conditions, circular camber is suggested although minor differences appear at leading and trailing edges. Experienced results showed these effects can be neglected. To simplify blade airfoil geometry representation, circular camber line was selected in this study instead of standard parabolic line. Thickness distribution of NACA 65 series [9] was used to profile blade suction and pressure side.

Figure 2 shows the singular arc camber used in this paper.

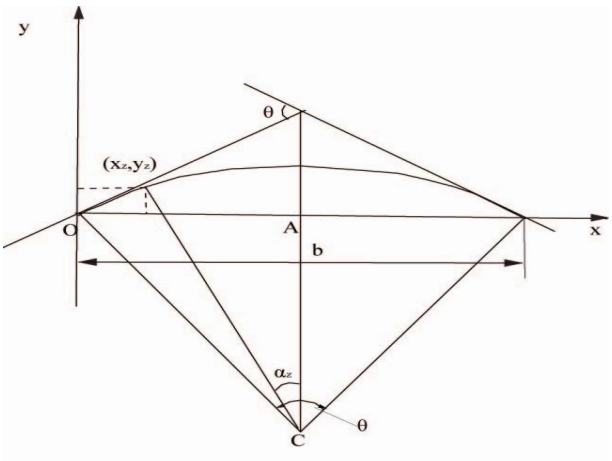

Fig. 2 Singular arc camber

The radius of camber arc is determined geometrically by the airfoil chord b and camber angle θ:

$$R = \frac{b}{2\sin\frac{\theta}{2}} \tag{2}$$

Camber shape is then profiled as:

$$\begin{cases} x_c = \dfrac{b}{2} - R \cdot \sin(\dfrac{\theta}{2} - \alpha_z) \\ y_c = R \cdot \cos(\dfrac{\theta}{2} - \alpha_z) - AC \end{cases} \tag{3}$$

With prescribed camber line, normal airfoil thickness distribution of NACA65-010 airfoils then imposed along the camber line. The suction side and the pressure side are calculated as following:

$$\begin{cases} x_s = \dfrac{b}{2} - (R + y_e) \cdot \sin(\dfrac{\theta}{2} - \alpha_z) \\ y_s = (R + y_e) \cdot \cos(\dfrac{\theta}{2} - \alpha_z) - AC \end{cases} \tag{4}$$

$$\begin{cases} x_p = \dfrac{b}{2} - (R - y_e) \cdot \sin(\dfrac{\theta}{2} - \alpha_z) \\ y_p = (R - y_e) \cdot \cos(\dfrac{\theta}{2} - \alpha_z) - AC \end{cases} \tag{5}$$

According to the systematic two-dimensional cascade tests of NACA 65-series compressor blades at low speeds [2], the deviation angle is determined by eq. (6). To form a working cascade, it is necessary to select right blade stagger angle. Stagger angle β_b is calculated as following:

$$\delta = 1.333 + 0.165\theta \tag{6}$$

$$\beta_b = \beta_2^* - \delta + \theta / 2 \tag{7}$$

Figure 3 shows the comparison of rotor and stator blade airfoils for NLF and HLF ones. Apparently, HLF has more cambered airfoils. Since blade axial chord length is limited to keep unchanged, HLF has reduced blade airfoil chord. Referred to eq. (1), new fan will have reduced solidity b/t which will contribute to the increasing diffusion factor. Therefore, the real diffusion factor of HLF is not only the result of increased blade airfoil camber. Airfoils of Fig. 3 were used to design HLF for 1000MW power generator of 1500rpm rotational speed. Its final design is an 1800-mm-diameter axial flow fan with blade height of 123mm and 1.9mm tip clearance. Since its small aspect ratio, straight blades were chosen for both rotor and stator for the sake of simple fabrication.

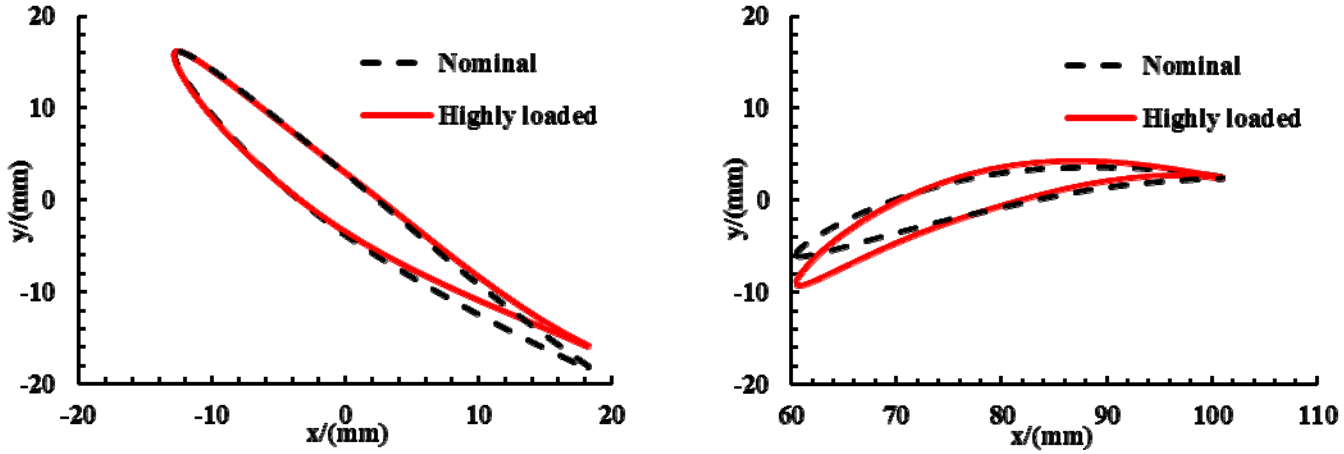

(A) Rotor (B) Stator

Fig. 3 Blade airfoils for NLF and HLF

3. Calculation method

To investigate the HLF performance numerically, the push-button CFD software FINETM Turbo by NUMECA International was applied. Reynolds-Averaged Navier-Stokes equations are solved in the finite-volume using explicit Runge-Kutta time-marching with implicit residual smoothing. Artificial viscosity by Jameson and multi-grid schemes are implemented to accelerate convergence rate [10]. It has been successful CFD software in compressor industry as in flow analysis [11, 12] and blade row aerodynamic optimal design [13, 14].

Flow was presumed to be steady and fully turbulent. Turbulence stress closure was k-ε two-equation model. To release the computation burden, extended near-wall function was used. The rotor/stator interaction was simulated by using quasi-steady mixing-plane model which averaged the flow properties at the rotor/stator interface [15]. For symmetry reasons, only one pitch of every blade row needed to be computed. The inlet boundary was set to standard ambient conditions. At the fan's discharge, the averaged static pressure was imposed to generate proper mass flow rate. Other boundaries were prescribed as no-slip wall or periodic boundary as its physical state. Steady blade speed line was calculated for alternative mass flow rate to draw out the performance characteristic line.

One stage of rotor and stator including the extended inlet and exit ducts were completely meshed in structured HOH topology. Each blade row had 41pitchwise×161axial×61spanwise points including those inside tip clearances. Limited study of grid dependency was carried out. Three basic grids were compared. They were coarse grid of 600,000 points, middle grid of 820,000 points and fine grid of one million. Comparisons of convergence rates, total residuals, mass flow rate errors, etc., middle level grid was chosen for its accuracy and relatively fast speed. In compliance with the k-ε turbulence model with extended wall-function, the values of y^+ were kept to 1 toward the solid surfaces, in order to achieve a reliable solution of the boundary layers. A midspan view of the mesh around blade airfoils is shown in Fig. 4.

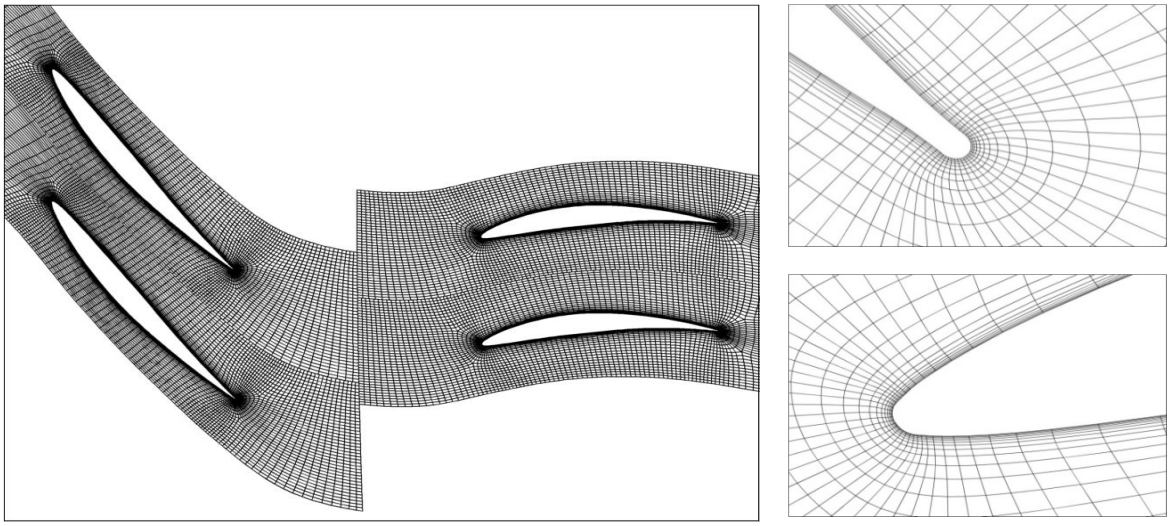

Fig. 4 Mesh for the highly loaded fan

4. Results and Discussion

4.1 Performance analysis

The efficiency and static pressure rise of the nominal stage and the newly designed highly loaded stage are shown in Fig. 5. Firstly, at design operation condition of flow coefficient $\phi = C_x / U_m = 0.52$, the static pressure rise from HLF is increased 20 percent with an efficiency decreased by 0.3 percent in value. It is not serious drawback for HLF design in which pressure increase is more valuable than efficiency deficit. Secondly, when the flow rate is larger than design, the efficiency tends to drop quickly. HLF is better than NLF. Thirdly, at small flow rate, HLF efficiency is lower than NLF.

One important feature in Fig. 5 is that the best operation point for HLF is moved toward larger flow rate, although the flow coefficient is kept the same in the stage velocity diagram as shown in Fig. 1. When the flow patterns from CFD results were examined, it was found that exit flow from rotor deviated from the designated direction which produced extra incidences to the downstream stator leading edges. At the exit of stator, flow deviated from blade airfoil surfaces. It can be concluded that fluid viscosity affects cascade flow to deviate from ideal stage design as shown in Figure 1. Correlations of flow deflection and losses are necessary to develop for HLF fans.

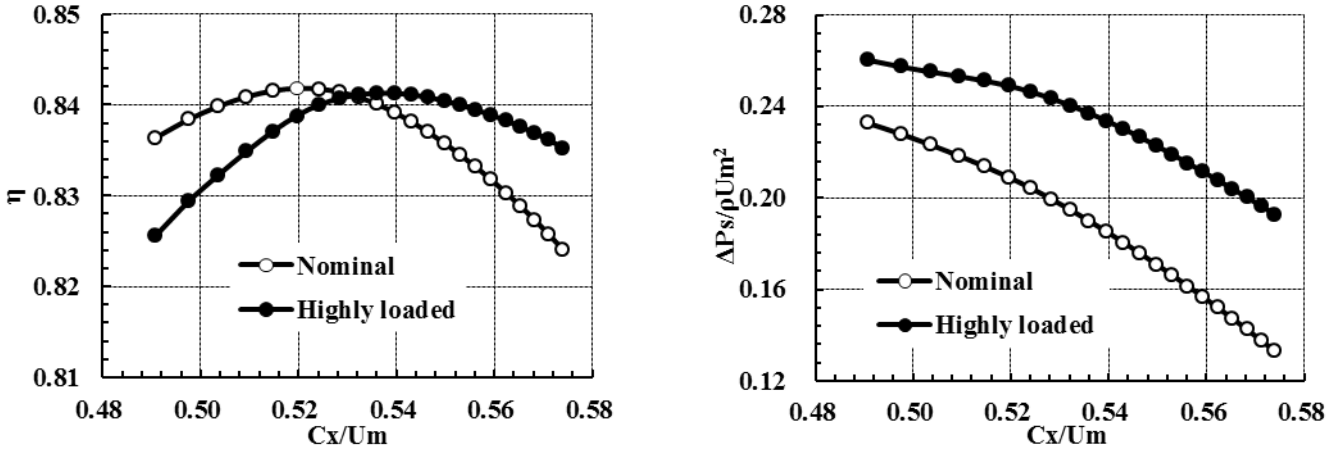

Fig. 5 Comparison of efficiency and static pressure rise

4.2 Flows in highly loaded rotor

Figure 6 shows the static pressure distributions along blade axial chord at 10 percent, 50 percent and 90 percent spanwise sections respectively. Across the rotor, corresponding diffusion factor was increased from 0.41 to 0.54, which was still less than the Lieblein critical value of 0.6. It seems reasonable to have little penalty on HLF rotor performance. The rotor work capacity of HLF is increased at the hub, the midspan and the tip. But adverse pressure gradient is strengthened at back of highly loaded rotor hub. The flow in rotor hub region separates approximately 60 percent of axial chord C_{Ax}.

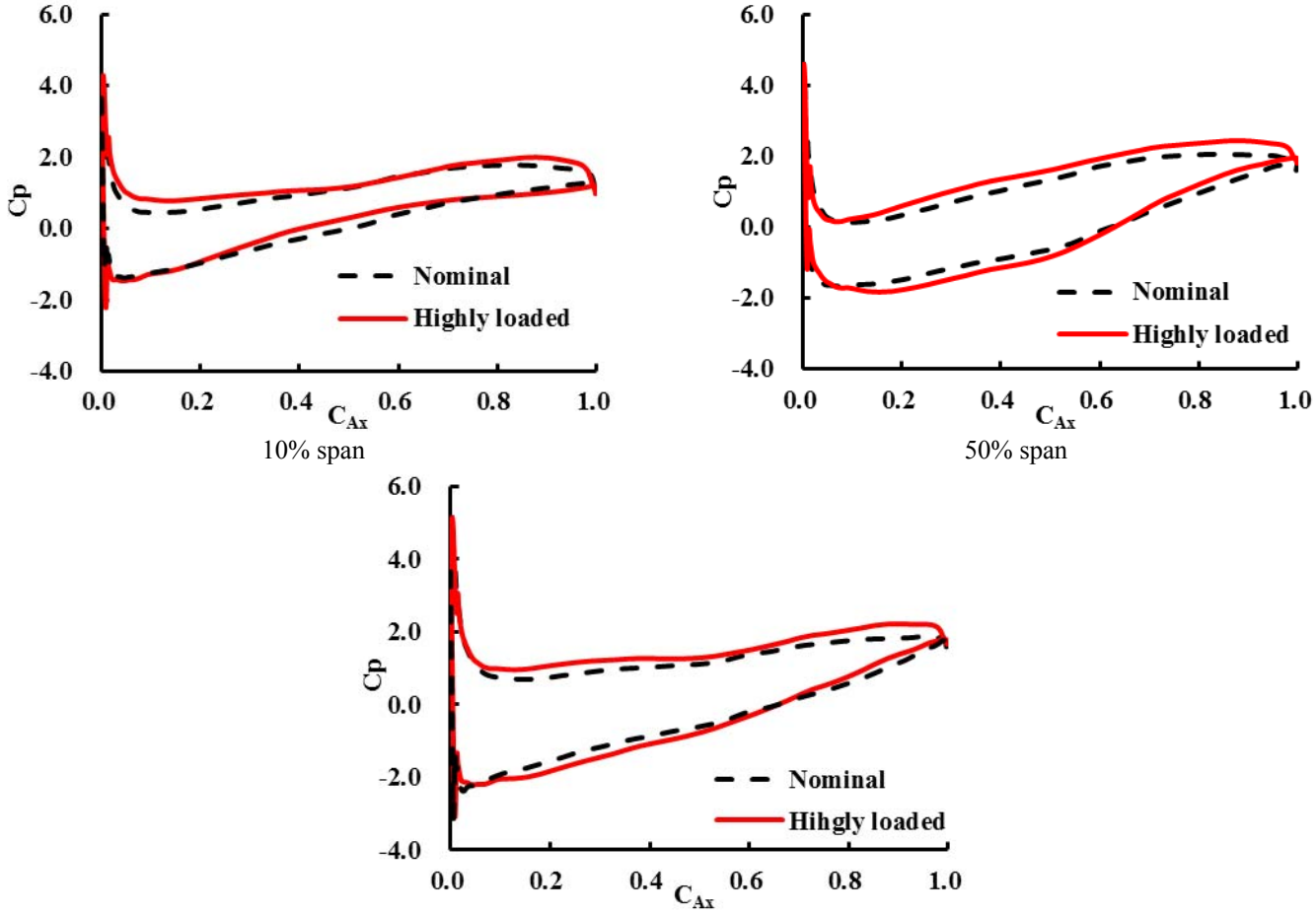

Fig. 6 Static pressure along rotor surface

Streamlines of the blade-to-blade flow at 10 percent, 50 percent and 90 percent spans are shown in Fig. 7, which demonstrate more clearly the flow patterns in both fan stages. Referring to Fig. 6, it is easy to find similar flow status in NLF and HLF rotors, except at the hub section where the flow in HLF shows a limited local separation zone close to the blade trailing edge. It generates an apparent wake flow which enters the downstream stator row. The rotor wake rushes onto stator leading edge and keeps developing through stator passage with little dispersion or diffusion along the stator blade suction surface. Due to the injection of low momentum fluid, the flow in hub-suction corner intends to be rolled up and lifted from hub surface.

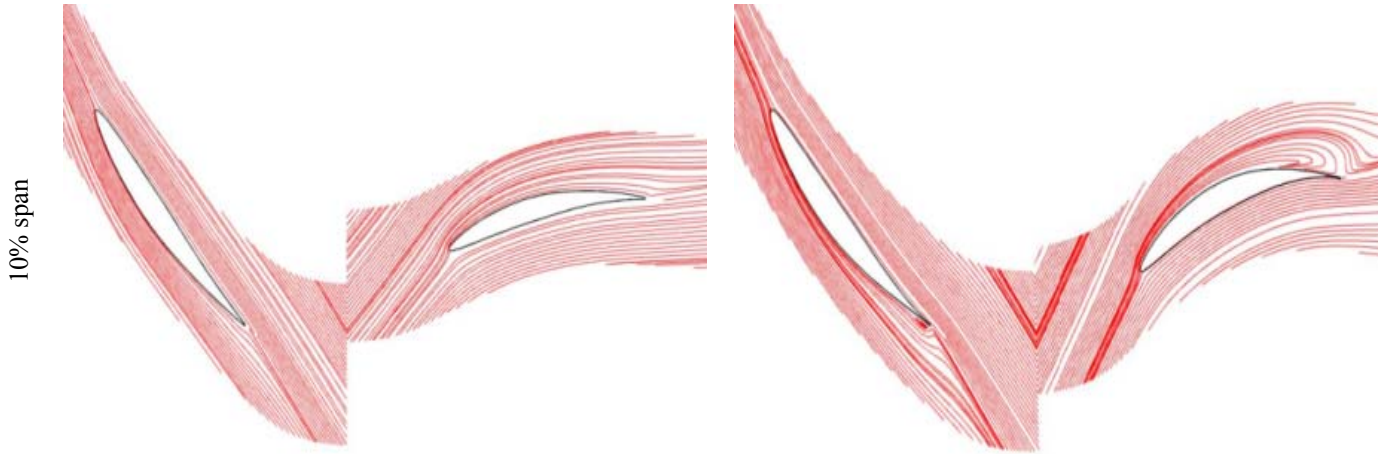

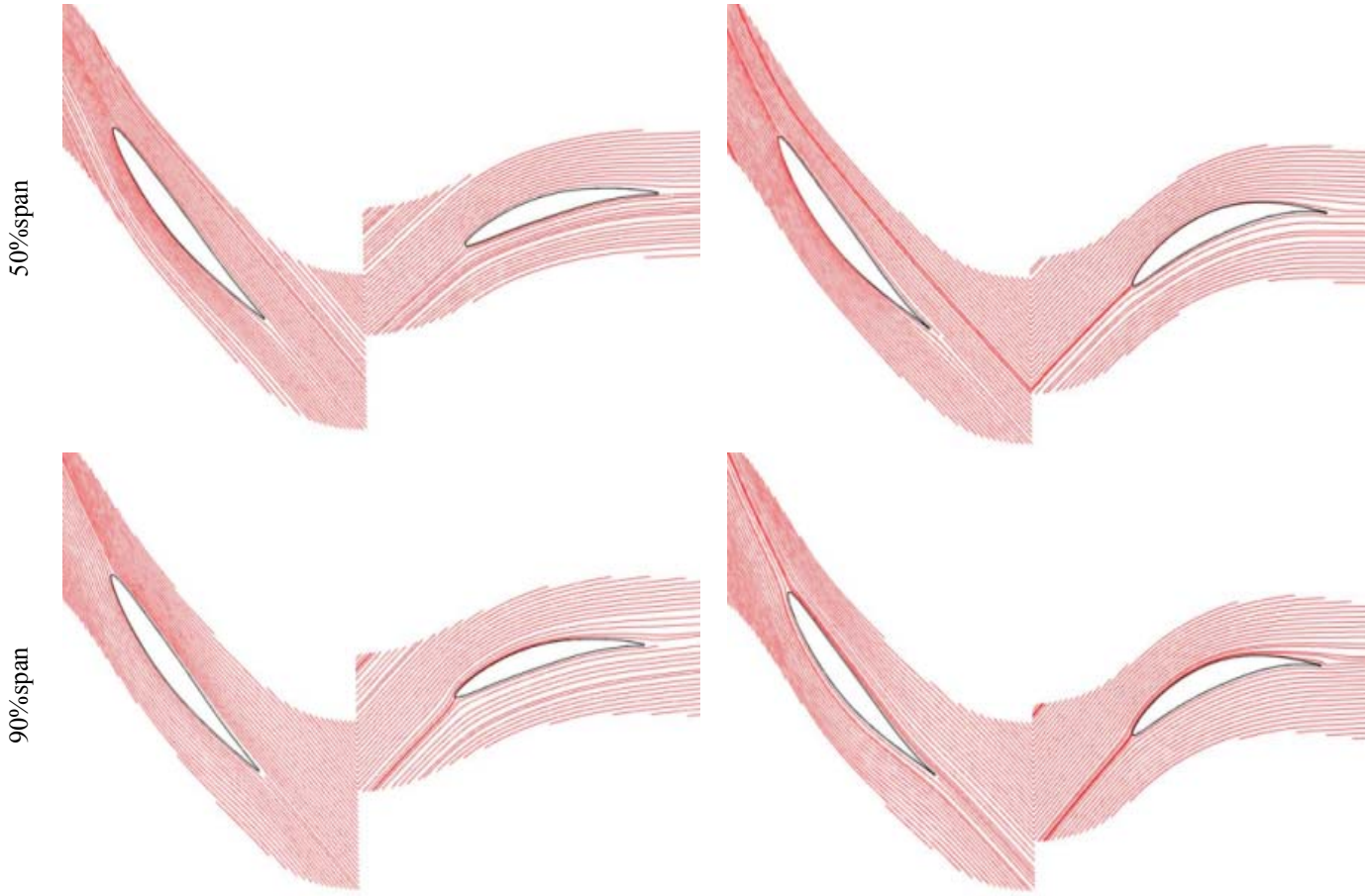

(A) Nominal loaded (B) Highly loaded

Fig. 7 Blade surface streamline

Fig. 8 shows the limited streamlines close to both rotor suction surfaces. Since the boundary layers on the endwall surfaces are low momentum fluids, it is difficult for those endwall flows to recover the pressure rise along with main flow diffusion. They are subjected to separation when they were approaching the trailing edge. Due to the blade rotation, separated hub flow does not keep stationary as common bubble-shaped blockage in two dimensional cascades, but rolled up toward midspan and merged with the main flow. When blade loading is increased, the area occupied by the rolled endwall flow becomes larger with higher strength in vorticity. At the blade tip region, local separation lines are also visible, because the rotors are unshrouded. Tip leakage flow is rolled down-wash into blade corner and merged with the main flow.

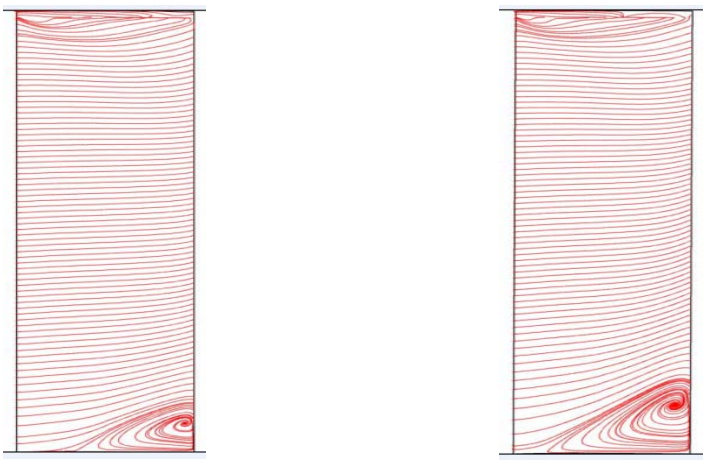

(A) Nominal loaded (B) Highly loaded

Fig. 8 Limited streamlines of rotor suction surface

Figure 9 shows the spanwise profile of pitched averaged energy loss coefficient at the rotor trailing edge. The rotor energy loss coefficient ϖ is defined by eq. (8), (9).

$$\varpi = \frac{\Delta I}{\rho U_{mid}^2} \tag{8}$$

$$I = CT_{stat} + \frac{W^2 + k - \omega^2 r^2}{2} \tag{9}$$

The largest loss core appears close to the rotor tip endwall due to the tip clearance. The energy losses of HLF rotor begin to exceed NLF one at 4 percent span. The largest difference occurs near 10 percent and 90 percent span locations. Hub corner stalling vortex as shown in Fig. 8 is responsible for the hub loss "bulb". Flow separation at the hub in NLF rotor starts at 40 percent of axial chord C_{Ax}, while in HLF rotor at 20 percent C_{Ax}. The areas of influence on radial flow in HLF rotor is nearly one and half times of NLF rotor. Therefore, the total flow loss in HLF rotor was increased. At midspan between 30 percent and 80 percent span range, special parabolic loss profile is formed by the increased diffusion factor along the blade span. However, when approaching the inter-boundary with endwall regions, flows are accelerated due to the blockage and alleviated flow loading.

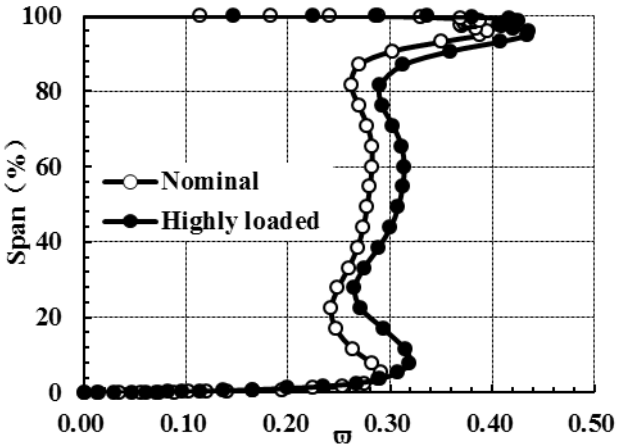

Fig. 9 Rotor energy loss coefficient along the spanwise

4.3 Flows in highly loaded stator

Figure 10 shows the static pressure distributions at 10 percent, 50 percent and 90 percent spanwise locations. On the stator surface, profiles of static pressure show different behaviors from hub to tip. At the hub, flow behaviors appear similar except the exit pressure is increased. At the midspan, HLF stator encloses a larger loading than NLF, and its largest pressure difference is moved from leading edge to 40 percent of axial chord. It has an evident effect that the streamwise pressure gradient along the aft part of stator blade is larger than NLF one which had effect to induce surface flow separation.

Compared with Fig. 7(B), it is interesting to note that although the static pressure profiles on stator surface are evidently different at mid and tip span, the blade-to-blade flow patterns did not show large differences. No clear flow separation is observed. It can then be argued that the large separation flow at hub should not be the result of the similar blade loading. It should be the result from the separation flow in the preceded rotor hub which changes the inlet flow condition with thickened inlet boundary layer.

In Fig. 11, it is shown the limited streamlines close to both stator suction surfaces. One distinct flow pattern is the three dimensional flows in the hub region. On NLF stator, the hub's local separation flow is constrained in the hub corner. But in HLF stator, the separation flow extends over 30 percent span at trailing edge which is a combined result of the enlarged rotor wake and the larger stator airfoil deflection.

In the stator tip region, it is clear that endwall secondary flow occurs due to the large flow turning. In the highly loaded fan, the stator's blade camber angle was 53°. Corresponding diffusion factor was 0.50, close to the Lieblein criteria. Therefore the three dimensional extension of endwall flow and separation lines resemble some endwall flow features in turbine cascade.

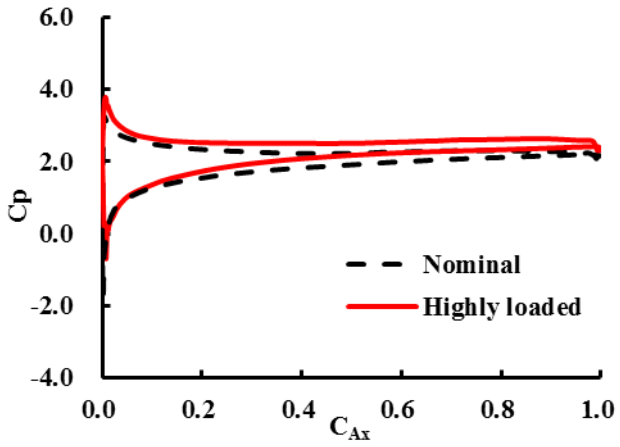

10% span

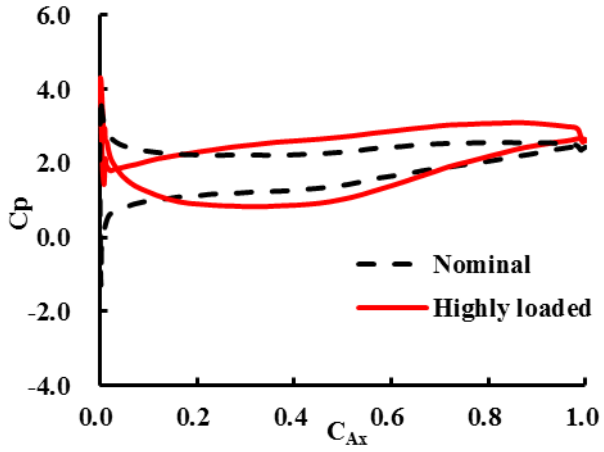

50% span

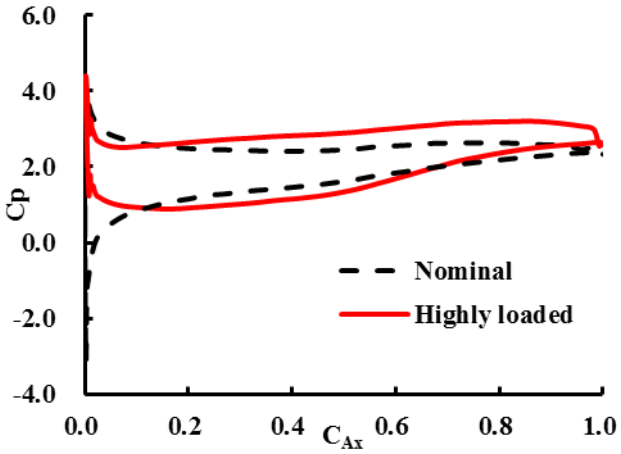

90% span

Fig. 10 Static pressure along rotor surface

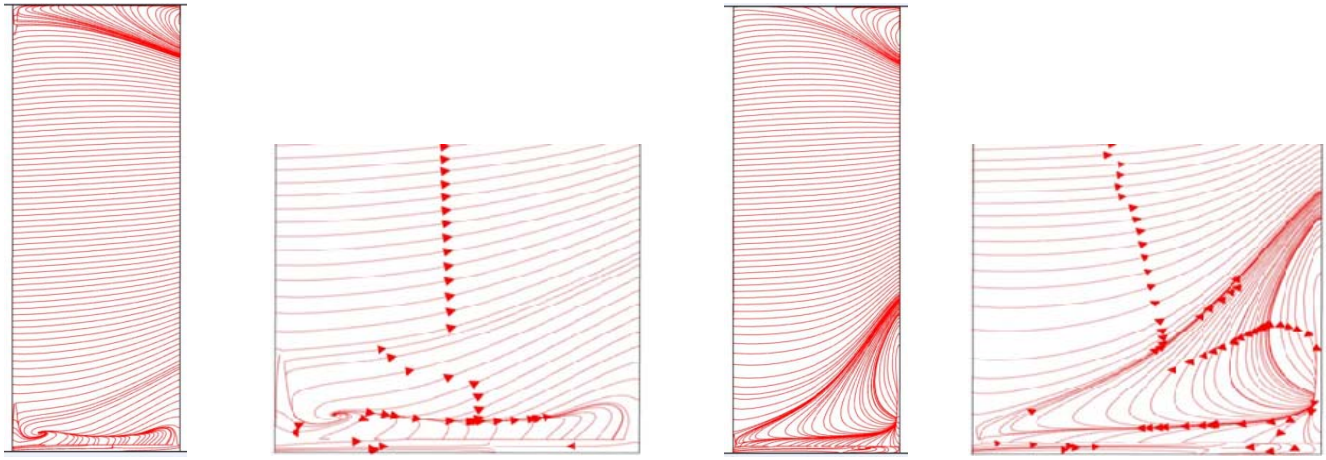

(A) Nominal loaded (B) Highly loaded

Fig. 11 Limited streamline of stator suction surface

It is illustrated in Fig. 12 the spanwise variation of pitch-averaged total pressure loss coefficient at the stator trailing edge. The stator total pressure loss coefficient ϖ_P was defined by eq. (10).

$$\varpi_p = \frac{P_{in}^* - P_{out}^*}{\rho U_{mid}^2} \tag{10}$$

The largest loss in stator appears in the bottom of the stator. It is generated due to the unshrouded stator hub clearance. The total pressure loss coefficient of the HLF stator begins to exceed the NLF stator at the 8 percent span and it reaches nearly twice at 20 percent span of NLF stator. It was shown that there were backflow on the suction surface at the hub in Fig. 11. The backflow is mixed with main stream impacting on the flow from 10 percent to 40 percent span as shown. This phenomenon also explains the stagnant stream in the HLF stator hub region which is shown in Fig. 7 (B). The change of the flow situation in the HLF rotor and the increased load on stator makes the flow conditions worse in HLF stator.

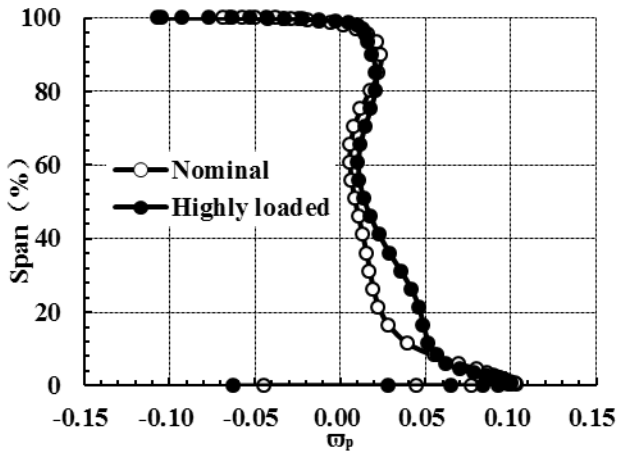

Fig. 12 Stator total pressure loss coefficient along the spanwise

5. Conclusions

It has been studied in this paper a design of highly load axial flow fan which had loading coefficient larger than 0.5. Its rotor and stator cascade diffusion factors were chosen close to Lieblein diffusion limitation. A baseline fan of the same flow coefficient with nominal loading factor of 0.42 was compared. Computational flow simulation was used to compare their performances and flow fields in the rotor and stator. It is concluded that:

(1) Highly loaded fan was realized by increasing the blade camber. Within the Lieblein limitation in diffusive flow, equivalent efficiency is possible to achieve for high loading factor close to 0.55. Due to the viscous effects in cascade flow, exit flow deflections become grown with increased blade loading. Optimal operation point was changed towards large flow rates.

(2) The flows in rotor and stator were distinctly three dimensional, especially in the hub region. In the rotor, hub endwall boundary layer flow was driven by the centrifugal force moving up towards the main flow. In the stator, the low momentum fluids from rotor hub were accumulated from blade mid-chord and separate along the rear airfoil. Large flow turning in stator induced them developing into the secondary flow similar to that in turbine cascade. Three dimensional flows of boundary layer fluids increased the flow losses in the cascade hub region.

(3) Main portion of the increased flow losses in highly load fan are attributed to the separated hub endwall flow due to blade rotation. It could not be solved in two dimensional cascade designing, such as low solidity of CDA airfoil. It is necessary to use three dimensional designing ideas, such as radial bowing, to control the radial pressure gradient to alleviate the radial flow in boundary layer.

Acknowledgments

The work in this paper gets supported by Leading Academic Discipline Project of Shanghai Municipal Education Committee, Project Number: J50501 and NSFC (50976072). Primary design and CFD computation was done by Mr Qian Jia. Authors would like to thank for their support and discussion of manuscript.

Nomenclature

b	Chord length[mm]	I	Rothalpy[J/kg]
θ	Bend angle[°]	ρ	Density [kg/m^3]
R	Radius of camber line[mm]	U_{mid}	Tangential velocity on the midspan[m/s]
C_{Ax}	Airfoil axial chord[mm]	C	Heat capacity at constant pressure [J/kg·k]
t	Pitch[mm]	T_{stat}	Static temperature[K]
β_1^*	Inlet flow angle(axial)[°]	W	relative velocity[m/s]
β_2^*	Outlet flow angle(axial)[°]	k	turbulent kinetic
δ	Deviation angle[°]	ω	rotor speed[r/min]
β_b	Stagger angle(axial)[°]	r	radius[mm]
C_x	Axial velocity[m/s]	ϖ_p	total pressure loss coefficient
φ	Flow coefficient	P_{in}^*	inlet total pressure[Pa]
C_p	Airfoil surface pressure coefficient	P_{out}^*	outlet total pressure[Pa]
ϖ	Energy loss coefficient		

References

[1] Wennerstrom A. J., 2000, Design of Highly Loaded Axial Flow Fans and Compressors, Concepts ETI, Inc., United States of America.

[2] Lieblein, S., 1965, "Experimental Flow in Two-Dimensional Cascades," Reprinted NASA SP-36: Aerodynamic Design of Axial Compressors, pp. 183-226.

[3] Emmerson P. R., 1998, "Three-Dimensional Flow Calculations of the Stator in a Highly Loaded Transonic Fan," Journal of Turbomachinery, Vol. 120, No. 1, pp. 141-146.

[4] Calvet W. J., Emmerson P. R., and Moore J. M., 2003, "Design, Test and Analysis of a High-pressure-ratio Transonic Fan," ASME Turbo Expo, Atlanta, Georgia, USA, GT2003-38302.

[5] Friedrichs J., Baumgarten S., Kosyna G., and Stark U., 2001, "Effect of Stator Design on Stator Boundary Layer Flow in a Highly Loaded Single-Stage Axial-flow Low-speed Compressor," Journal of Turbomachinery, Vol. 123, No. 3, pp.483-489.

[6] Sonoda T., Yamaguchi Y., Arima T., et al, 2004, "Advanced High Turning Compressor Airfoils for Low Reynolds Number Condition—Part I: Design and Optimization," Journal of Turbomachinery, Vol. 126, pp. 350-359.

[7] Schreiber H., Steinert W., Sonoda T., and Arima T., 2004, "Advanced High-Turning Compressor Airfoils for Low Reynolds Number Condition—Part Ⅱ: Experimental and Numerical Analysis," Journal of Turbomachinery, Vol. 126, pp. 482-492.

[8] Dickens T., Day I., 2011, "The Design of Highly Loaded Axial Compressors," Journal of Turbomachinery, Vol. 133, 031007.

[9] Herrig L. J., Emery J. C., and Erwin J. R., 1957, "Systematic Two-Dimensional Cascade Tests of NACA 65-series Compressor," NASA TN-3916.

[10] NUMECA Int., 2003, "NUMECA's Flow Integrated Environment for Turbomachinery and Internal Flows", User Manual version 6.1-1, NUMECA Int., Brussels, Belgium.

[11] Kang Sh. Hirsch C., 1996, “Numerical Simulation of Three-Dimensional Viscous Flow in a Linear Compressor cascade with Tip Clearance,” Journal of Turbomachinery, Vol. 118, No. 3, pp. 492-505.
[12] Fischer A., Riess W., Seume J. R., 2003, “Performance of Strongly Bowed Stators in a 4-Stage High Speed Compressor,” ASME Turbo Expo, Atlanta, Georgia, USA, GT2003-38392.
[13] Luo C., Song L., Li J. and Feng Z., 2012, “A Study on Multidisciplinary Optimization of an Axial Compressor Blade Based on Evolutionary Algorithms, Journal of Turbomachinery, Vol. 134, No. 5, 054501.
[14] Wang X.D, Hirsch C., Kang Sh., and Lacor C., 2011, “Multi-Objective Optimization of Turbomachinery Using Improved NSGA-II and Approximation Model,” Computer Methods in Applied Mechanics and Engineering, Vol. 200, No. 9-12, pp. 883-895.
[15] Cumpsty, N. A., 1989, Compressor aerodynamics, Chapman and Hall, London.